Antenna Servo Control System Characterization: Rate Loop Analysis for 34-m Antenna at DSS 15

J. A. Nickerson, D. G. Cox, H. K. Smith, J. H. Engel, and H. G. Ahlstrom
Ground Antenna and Facilities Engineering Section

This report characterizes the elevation and azimuth servo rate loops at the 34-m High Efficiency Deep Space Station 15 (DSS 15). Time and frequency response performance criteria were measured. The results are compared to theoretically deduced performance criteria. Unexpected anomalies in the frequency response are observed and identified.

I. Introduction

This report is the first in a series of reports aimed at studying and characterizing antenna drive control system components of the Deep Space Network antennas. Three types of antennas will be characterized: (a) the high efficiency 34-meter AZ/EL antenna at Deep Space Station 15 (DSS 15), (b) the 34-meter HA/DEC antenna at DSS 12, and (c) the 64/70-meter AZ/EL antenna at DSS 14.

Two major control loops of the antenna control system are the position loop and rate loop. The position loop drives the antenna based on a desired angle command. Figure 1 is a functional block diagram of a typical position control loop. A major component of the position loop is the rate loop. The rate loop is a feedback control system designed to control motor angular velocity. It responds to a motor rate command signal issued from the position loop. Characterization of an antenna's motion control system requires operational knowledge of both the position and rate loops.

Standard control system performance criteria include frequency and time domain characteristics. The frequency response of a system, typically displayed in a Bode plot, depicts system response in terms of gain and phase lag as a function of frequency. Control system bandwidth is deduced from Bode plots. Typical time domain characteristics describe system dynamics in response to a unit step command. Time domain measurements include rise time, percent overshoot, and settling time (see Ref. 1).

This report presents a frequency response characterization of azimuth and elevation rate loops of the 34-meter antenna at DSS 15. Also, normalized rate loop step responses are presented and discussed. Empirical results are compared to theoretical responses derived from linear mathematical models. Subsequent reports will analyze the position loop for the same antenna and extend control system analysis to other antennas in the Deep Space Network (DSN).

II. Rate Loop Model

A rate loop is closed around each drive motor using a tachometer as a feedback transducer. The simplified functional block diagram, using Laplace domain models, is presented in Fig. 2. The functional blocks around the simplified loop are: rate loop compensation, a current loop, motor load and

tachometer scaling. The K's represent gain and conversion factors, τ's represent time constants of various components, and the J represents motor inertia. Elevation and azimuth models are identical in form but encompass different coefficient values.

The frequency response of elevation and azimuth rate loops is shown in Figs. 3 and 4, respectively. These frequency responses were generated from the model in Fig. 2 using constants supplied by the manufacturer. The frequency response of the elevation rate loop has a maximum gain of 1.2 dB at 2.2 Hz. Beyond 2.2 Hz the gain rolls off with increasing negative slope until near 20 Hz, the roll off is −40 dB per decade. The gain bandwidth is 9.1 Hz. The phase lag is small for low frequencies and monotonically decreases as a function of frequency. The azimuth rate loop frequency response is similar to the elevation rate loop and has a bandwidth of 9.4 Hz.

The same mathematical models were used to simulate the rate loop time response to a unit step input. Figures 5 and 6 show elevation and azimuth rate loop responses to a unit step. For each axis's rate loop, the rise time and settling time are the same at 0.09 seconds and 0.30 seconds, respectively. The percent overshoot for the elevation loop was 4.0%, which is slightly different from 4.5% for the azimuth axis. Both the low percent overshoot and fast rise time, which the mathematical models suggest, are desirable qualities for a good pointing and tracking control system.

III. Experimental Procedures

At the DSS 15 antenna site each rate loop was disconnected from the position control computer and connected to the signal generator of a frequency response analyzer. A scaled tachometer feedback voltage was connected to the analyzer. The servo rate loop was driven with a sinusoidal voltage from the signal generator of the frequency analyzer at many frequencies selected to cover the range desired (0.1 – 20 Hz). The amplitude of the tachometer voltage and its phase lag at each frequency were reported by the analyzer and recorded.

In the first set of tests two types of input signals were used to measure the frequency response: (a) a biased sinusoidal input voltage, and (b) an unbiased sinusoidal input voltage. The sinusoidal voltage varied between ±0.06 volts (corresponding to an antenna angular velocity of ±5 mdeg/s). The bias was 0.12 volts (corresponding to an antenna angular velocity of 10 mdeg/s). Tests were conducted on the elevation rate loop centered around four elevation angles: 7, 45, 70, and 88 degrees. Azimuth rate loop tests were conducted at three elevation angles: 7, 45, and 88 degrees. Only one azimuth angle was tested since the azimuth axis inertia changes only with elevation angle. The elevation angle was varied during azimuth tests to check for cross coupling and effects due to changing inertia.

The second set of tests was performed which measured the step response of both rate loops. For these tests a portable computer with digital-to-analog (D/A) and analog-to-digital (A/D) conversion capabilities was used. A voltage step was induced into the rate loop using the D/A converter, and the scaled tachometer voltage was recorded by the computer using the A/D converter. The rate loop response was sampled and digitized 50 times/second.

IV. Results

A total of eight frequency tests was made on both axes: four with biased input signals and four with no bias. A Bode plot was generated for each test as shown in Figs. 5 through 19.

A. Biased Input Tests — Elevation Loop

Figures 7, 8, 9, and 10 give the results of a biased sinusoidal input voltage for the elevation rate loop. Each was made at four different elevation angles. All four tests had similar results and indicate that the frequency response of the rate loop is not a function of elevation angle. Two abnormalities are seen in the frequency response of Figs. 7 through 10. The first is that a large anti-resonance (inverted resonance) appears in the neighborhood of 2.3 Hz. A second smaller anti-resonance appears near 3.4 Hz. These anti-resonances are seen in both magnitude and phase plots.

The large anti-resonance is believed to be the first mode of torsional vibration between the motor's rotor inertia and the antenna's inertia. This two-degree of freedom system is idealized as two inertias (or masses) connected by a spring. The antenna and the motor rotor are the two inertias while the gear reducer acts as the spring. The inertia of the antenna, as seen by each elevation motor, is reported to be 0.01898 kg-m^2 (0.014 lb-ft-s^2). The motor and gearbox inertia, as seen by the motor, is 0.141 kg-m^2 (0.104 lb-ft-s^2). The spring constant of the gear reducer is nonlinear and ranges between 3.96 N-m/rad (1.71 lb-ft/rad) and 5.33 N-m/rad (3.93 lb-ft/rad) for torque values less than 25% maximum motor torque. Equation (1) calculates the fundamental natural frequency, w_n, for a two mass torsional system connected by a spring, where K_s is the torsional stiffness of the gear reducer, J_1 is the inertia of the motor's rotor, and J_2 is the antennas's inertia as seen by the motor (see Ref. 2):

$$w_n = \sqrt{K_s (J_1 + J_2) / (J_1 J_2)} \qquad (1)$$

Using the above values for J_1, J_2, and K_s suggests the first mode of torsional oscillation is between 1.87 Hz and 2.84 Hz. The large 2.3-Hz anti-resonance frequency is centered between the two frequencies; therefore, it is reasonable to assume that the large anti-resonance is due to this first torsional oscillatory mode.

Note that during first torsional mode vibrations, a motionless node exists on the flexible link between the two inertias. The greater the ratio of inertias the closer the node is to the larger inertia. This indicates that the motion of the larger inertia (which is the motor's rotor) is attenuated. The second small anti-resonance located near 3.4 Hz is also believed to be due to a torsional mode of vibration. This has not, however, been verified.

The frequency responses shown in Figs. 7, 8, 9, and 10 can also be compared with the theoretical frequency response shown in Fig. 3. The theoretical frequency response does not contain the anti-resonances found in the experimental data since these are not accounted for by the model. The actual frequency responses have slightly lower phase and gain margins compared to the theoretical frequency response shown in Fig. 3. The actual bandwidth is 8.8 Hz, which is 4% less than the theoretical bandwidth.

B. Unbiased Input Tests — Elevation Loop

Figures 11, 12, 13, and 14 show results from the elevation axis rate loop using an unbiased sinusoidal input voltage instead of a biased voltage. Three observations were made from these results: the frequency response is completely different from biased tests yet the same large and small anti-resonances are still observed and the frequency response is not a function of elevation angle. The rate loop bandwidth is reduced from 3.8 Hz to 1 Hz. This is a 90% decrease in bandwidth. Greater phase lag also exists below 3 Hz. One cause of the bandwidth and phase lag behavior could be the susceptibility of the system to friction; the friction occurring when the motors change direction. Changing motor direction reduces rate loop performance.

C. Biased Input Tests — Azimuth Rate Loop

The tests performed on the elevation axis were repeated on the azimuth axis. The results from biased input are plotted in Figs. 15, 16, and 17. The tests were performed at the three elevation angles of 7, 45, and 88 degrees, respectively. Again, the frequency response was found not to be a function of elevation angle. All three frequency responses are similar; but comparisons between the experimental results and theory show a significant difference. The measured rate loop bandwidth is greater than what theory predicts. A 27% increase is seen from 9.4 Hz to 12 Hz. Analyzing phase margin yields similar comparisons. A small dip was observed in the gain at 2 Hz in all three Bode plots; otherwise, no large anti-resonances were observed. The first mode is calculated from the azimuth axis inertias, J_1 = 0.123 kg-m^2 (0.0907 lbf-ft-s^2) and J_2 = 0.0118 kg-m^2 (0.0087 lbf-ft-s^2). In the azimuth axis, four motors share the load instead of two as in the elevation axis. Assuming that each motor operates below 12.5% of maximum torque, the nonlinear spring constant ranges between 0.468 N-m/rad (0.345 ft-lbf/rad) and 3.23 N-m/rad (2.38 ft-lbf/rad). This corresponds to a natural frequency between 1.12 and 2.76 Hz. The small anti-resonance at 2.0 Hz is centered between these calculated frequencies. The anti-resonance is not as significant, however, as in the elevation axis. This may be due to cross coupling and structural damping between axes. An additional test using double the biased voltage and double the sinusoidal voltage amplitude was made to further investigate the anti-resonance reported above. Figure 18 presents the results of this test. The anti-resonance is pronounced during this test and validates prior observations.

D. Unbiased Input Test — Azimuth Rate Loop

Three additional tests were performed on the azimuth axis using an unbiased sinusoidal input voltage with the elevation axis at angles 7, 45, and 88 degrees. The empirical Bode plots shown in Figs. 19, 20, and 21 indicate dramatic gain attenuation and phase lag at low frequencies and that the frequency response is not a function of elevation angle. Gain attenuation and phase lag are attributed to friction, backlash, and drive-associated nonlinearities. The contributions of each type of nonlinearity to the frequency response have not been determined. The frequency responses in Figs. 19, 20, and 21 are very different from the theoretical prediction shown in Fig. 4.

E. Step Responses

Step response tests were performed on both elevation and azimuth rate loops. Normalized tachometer voltage is presented as a function of time in Figs. 22 and 23. The rise time and settling time of the elevation rate loop, 0.12 seconds and 0.37 seconds, respectively, are more than 20% longer than the predicted values shown in Fig. 5. The measured rate loop response gave a 1% overshoot compared to the 4% predicted overshoot.

The azimuth rate loop step response had similar characteristics to the elevation rate loop: rise time = 0.13 seconds; settling time = 0.34 seconds; percent overshoot = 0%. Again, the measured rise time and settling time are more than 20% longer than the predicted values in Fig. 6. Both the low percent overshoot and fast rise time exhibited by the rate loops are desirable performance characteristics.

V. Conclusions

The frequency response of elevation and azimuth rate loops had several anomalies. Anti-resonances existed in both elevation and azimuth rate loops. These resonances were deduced to be fundamental torsional modes of vibration between the antenna and motor inertias. The calculated elevation axis torsional natural frequency between 1.87 Hz and 2.84 Hz was in good agreement with the observed resonance at 2.3 Hz. The calculated azimuth axis natural frequency between 1.12 Hz and 2.76 Hz was also in good agreement with the observed resonance at 2.0 Hz.

System bandwidth of elevation and azimuth rate loops, based on a biased input voltage, was 8.8 Hz and 12 Hz, respectively. These were similar to the predicted bandwidths of 9.1 Hz and 9.4 Hz. Using an unbiased sinusoid voltage seriously degraded system bandwidth performance in the elevation axis by almost 90%. Unbiased voltage tests in the azimuth axis indicated that large nonlinearities exist such as friction, backlash, and other drive-associated nonlinearities.

Step response characterization tests indicate elevation and azimuth rate loops have fast rise times (less than 0.13 seconds), low or no overshoot, and settling times less than 0.4 seconds. These performance characteristics indicate that the rate loops respond well to command voltages.

Both frequency and step response characterization indicate the linear mathematical model of the rate loop does not accurately describe system dynamics.

References

1. Dorf, R. C., *Modern Control Systems*, 3rd ed., Addison-Wesley, Reading, Mass., 1983.
2. Baumeister, T., Avallone, E. A., and Baumeister III, T., *Mark's Standard Handbook for Mechanical Engineers*, 8th ed., McGraw-Hill, New York, 1978.

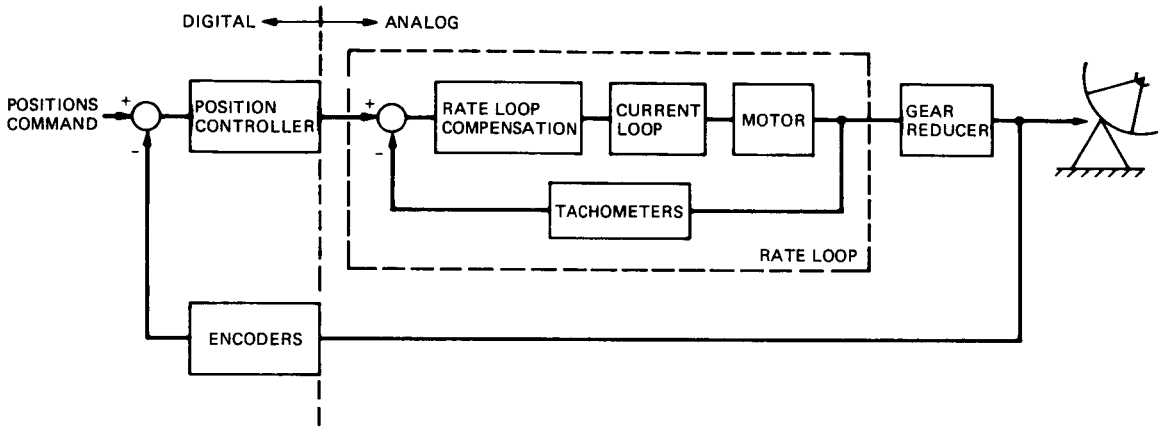

Fig. 1. Position loop

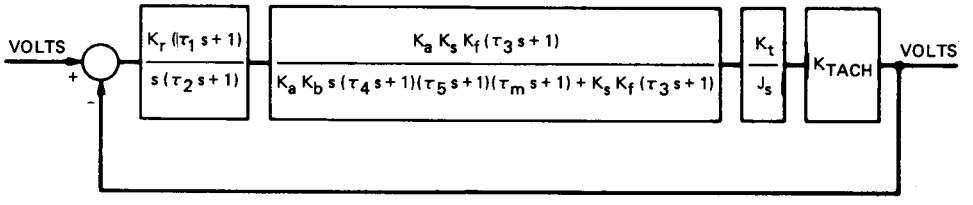

Fig. 2. Rate loop

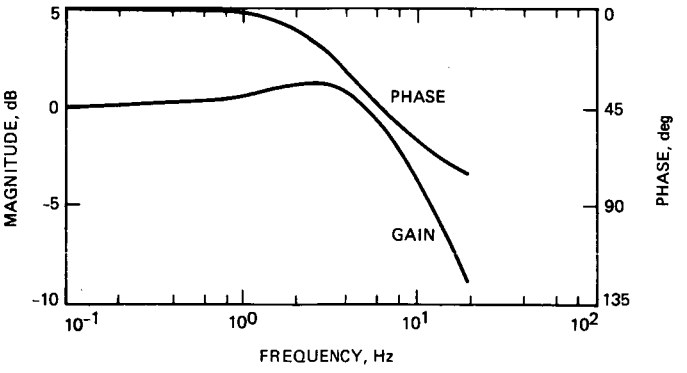

Fig. 3. Simulated frequency response of the elevation rate loop model, DSS 15 antenna

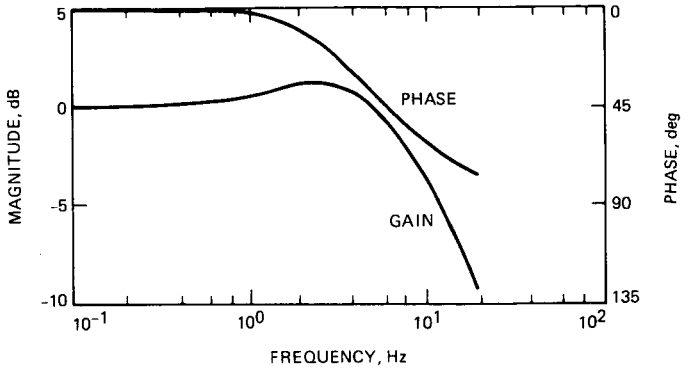

Fig. 4. Simulated frequency response of the azimuth rate loop model, DSS 15 antenna

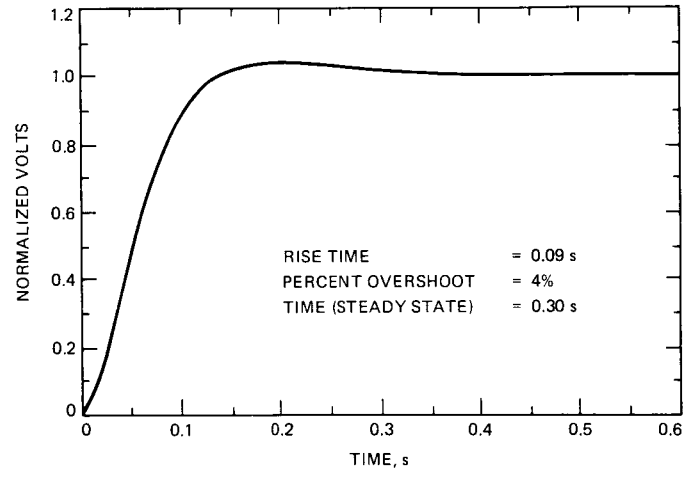

Fig. 5. Simulated step response — elevation rate loop model, DSS 15 antenna

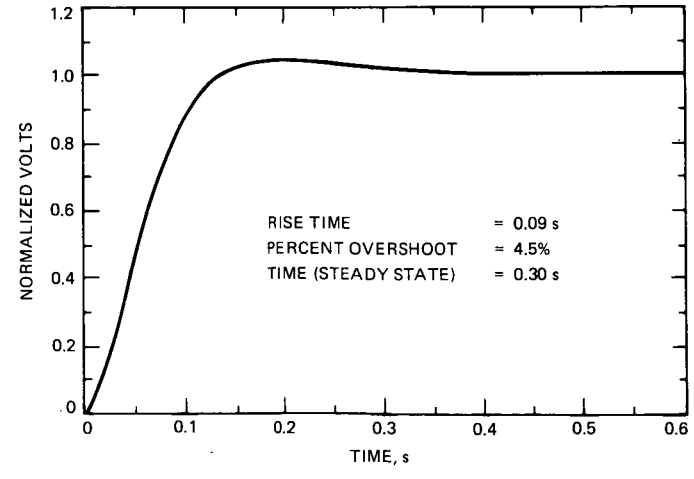

Fig. 6. Simulated step response — azimuth rate loop model, DSS 15 antenna

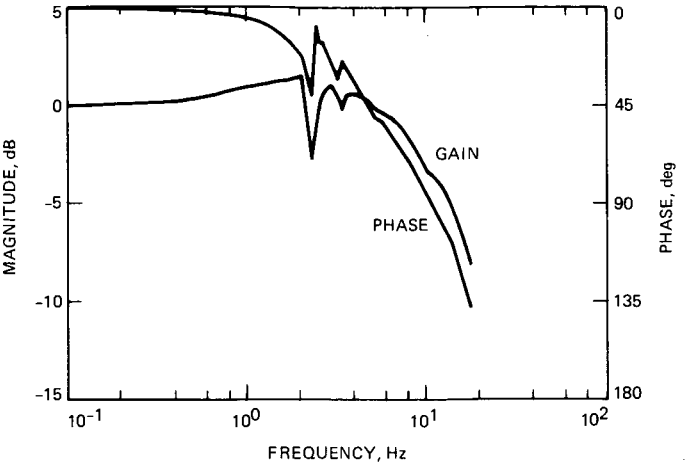

Fig. 7. Biased input test — elevation axis loop, EL = 7 deg

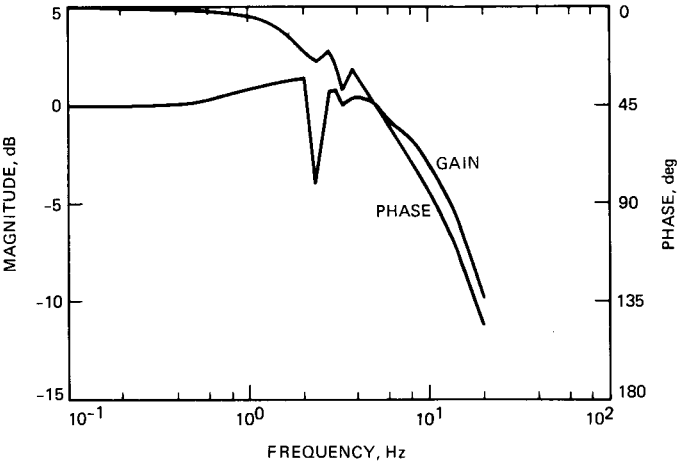

Fig. 8. Biased input test — elevation axis loop, EL = 45 deg

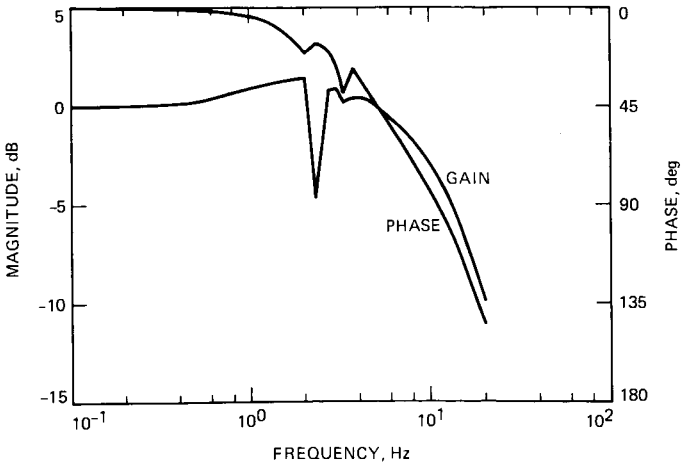

Fig. 9. Biased input test — elevation axis loop, EL = 70 deg

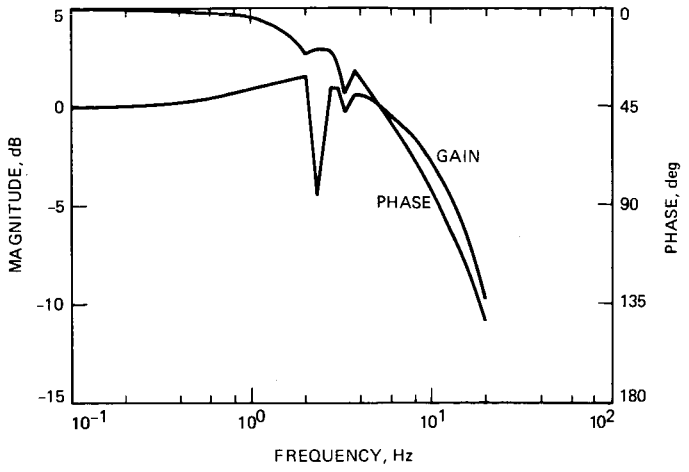

Fig. 10. Biased input test — elevation axis loop, EL = 88 deg

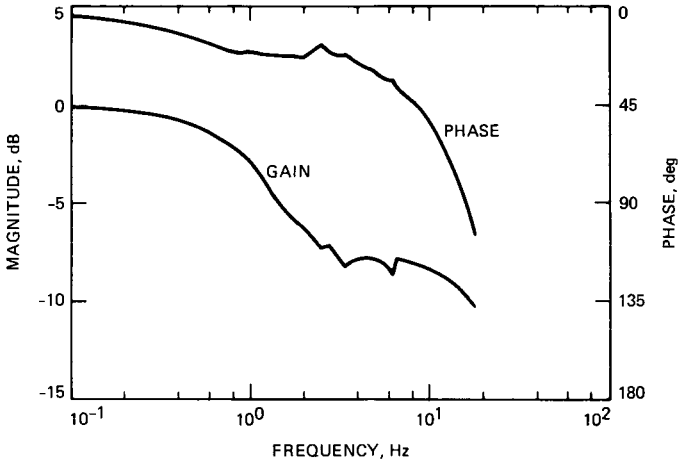

Fig. 11. Unbiased input test — elevation axis loop, EL = 7 deg

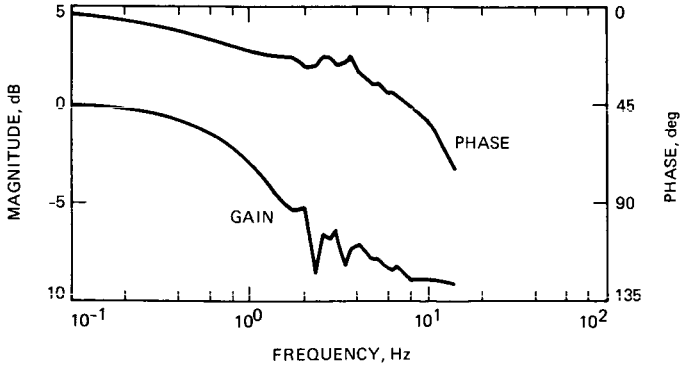

Fig. 12. Unbiased input test — elevation axis loop, EL = 45 deg

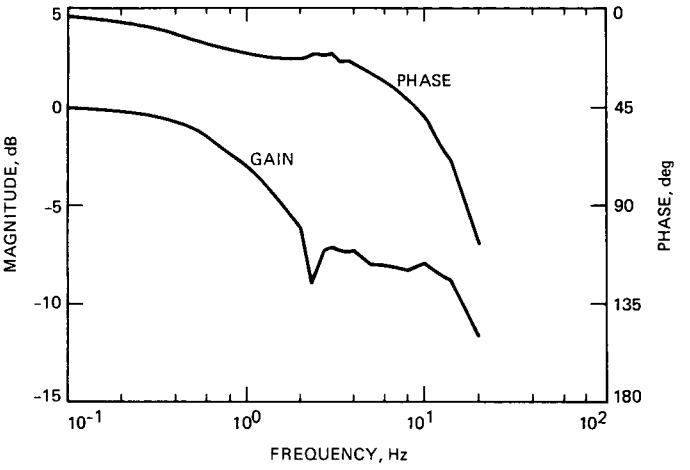

Fig. 13. Unbiased input test — elevation axis loop, EL = 70 deg

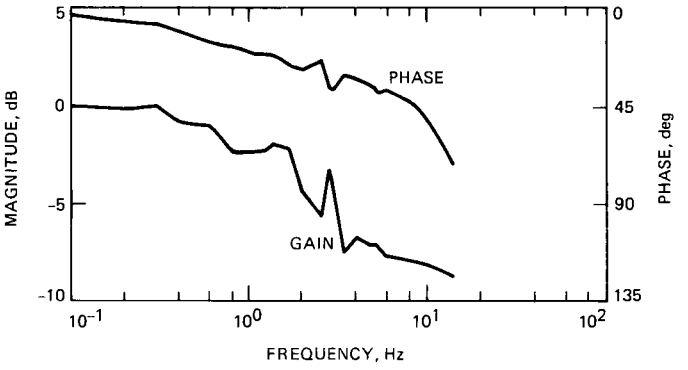

Fig. 14. Unbiased input test — elevation axis loop, EL = 88 deg

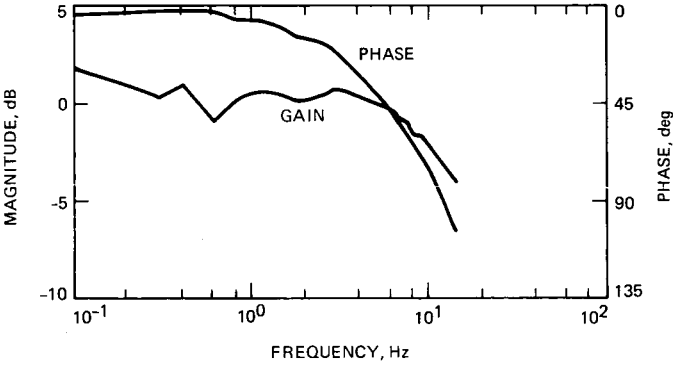

Fig. 15. Biased input test — azimuth axis loop, EL = 7 deg

C-3

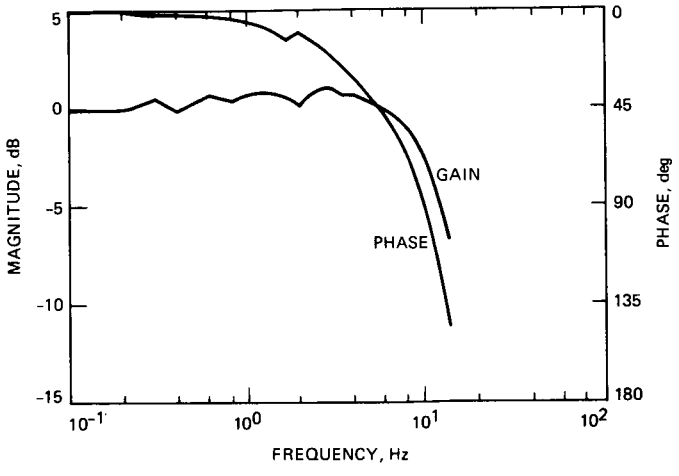

Fig. 16. Biased input test — azimuth axis loop, EL = 45 deg

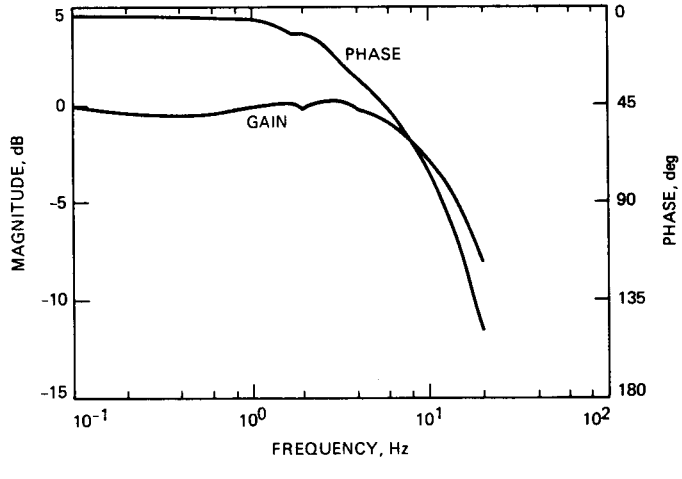

Fig. 17. Biased input test — azimuth axis loop, EL = 88 deg

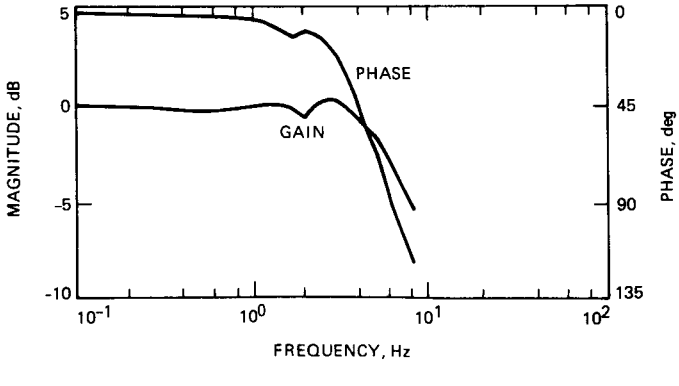

Fig. 18. Double input and double bias test — azimuth axis loop, EL = 45 deg

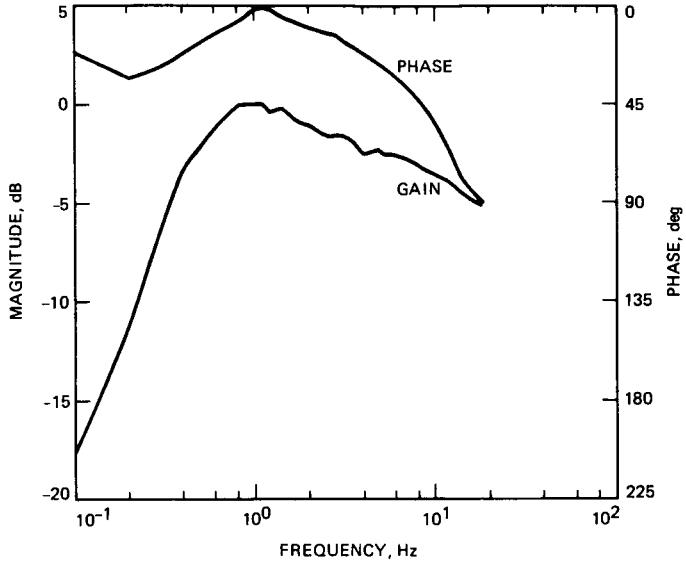

Fig. 19. Unbiased input test — azimuth axis loop, EL = 7 deg

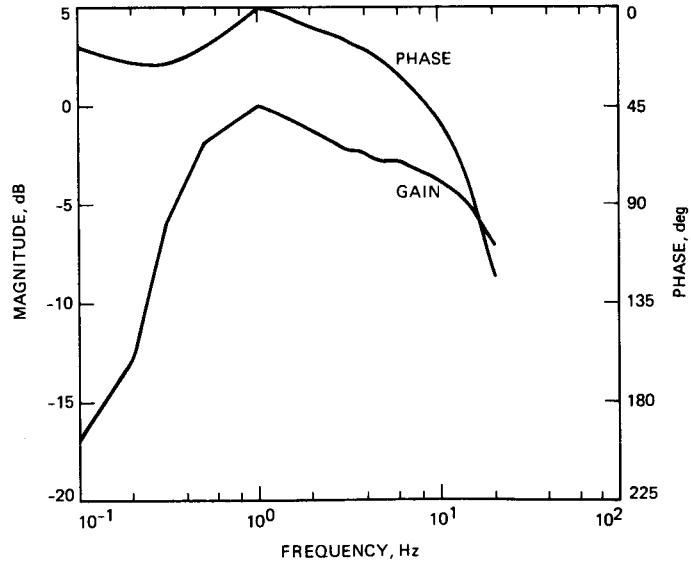

Fig. 20. Unbiased input test — azimuth axis loop, EL = 45 deg

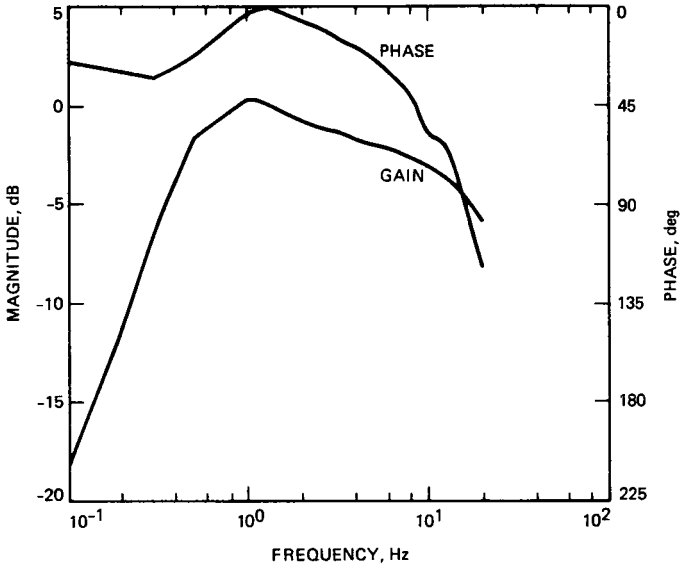

Fig. 21. Unbiased input test — azimuth axis loop, EL = 88 deg

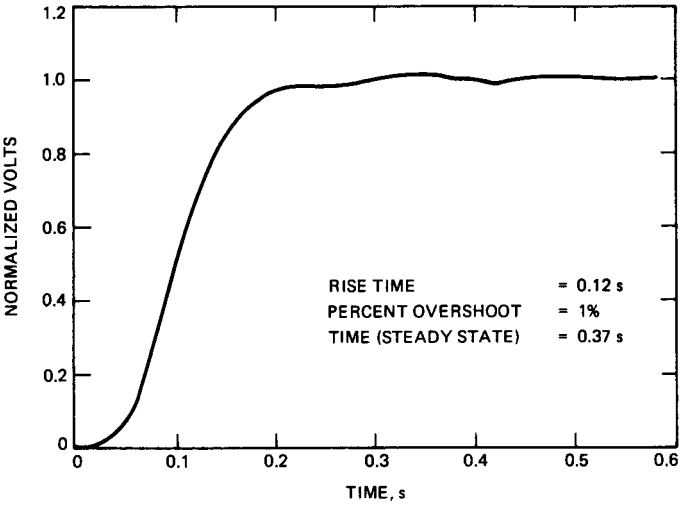

Fig. 22. Actual step response — elevation axis loop, DSS 15

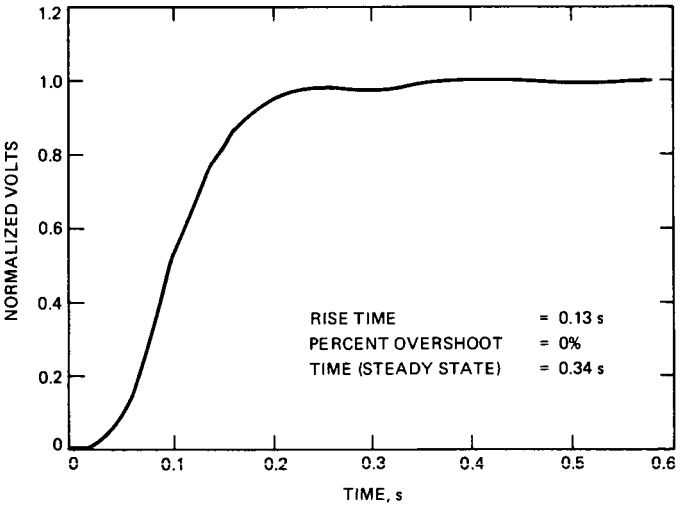

Fig. 23. Actual step response — azimuth axis loop, DSS 15